IEEE Access
Multidisciplinary ⋮ Rapid Review ⋮ Open Access Journal

Received November 15, 2019, accepted November 22, 2019, date of publication November 27, 2019,
date of current version December 13, 2019.

Digital Object Identifier 10.1109/ACCESS.2019.2956190

Finite-Time Control of Multirotor UAVs Under Disturbances

WONMO CHUNG[1], DIPAK KUMAR GIRI[2], AND HUNGSUN SON[1], (Member, IEEE)
[1]School of Mechanical, Aerospace and Nuclear Engineering, Ulsan National Institute of Science and Technology, Ulsan 44919, South Korea
[2]Department of Aerospace Engineering, Indian Institute of Technology at Kanpur, Kanpur 208016, India

Corresponding author: Hungsun Son (hson@unist.ac.kr)

This work was supported in part by the Future Innovation Research Fund of Ulsan National Institute of Science and Technology (UNIST) under Grant 1.190003.01, in part by the Development of Multi-degrees of Freedom Spherical Motion Platform under Grant 2.190080.01, in part by the Development of Drone System for Ship and Marine Mission of Civil Military Technology Cooperation Center under Grant 2.180832.01, in part by the National Research Foundation of Korea (NRF) of the Korean National Police Agency under Grant 2018M3E2A1081549, and in part by the Ministry of Science and ICT for Police Field Customized Research and Development Project.

ABSTRACT A new finite-time control method based on a sliding mode for a multirotor unmanned aerial vehicle (UAV) is developed to improve both the transient and steady-state responses, including overshoot and steady-state error in the presence of uncertainties and external disturbances. First, a virtual control with nonlinear sliding manifolds is designed to achieve position-tracking capability, as well as to guarantee the fast convergence of the UAV to a desired position. Furthermore, an ultimate control is developed for the desired attitude-tracking performance. Various uncertainties, including torque due to the discordance between the centre of mass and rotation and wind disturbances are considered. The Lyapunov stability theorem is then applied step-by-step to prove the asymptotically stable and finite-time convergence in position and attitude controllers. Second, the proposed controller is implemented in an open-source hardware platform for a quadrotor UAV. Both numerical and experimental results are compared to validate the tracking performance for attitude and position control, as well as robustness under disturbances.

INDEX TERMS Finite-time control, sliding-mode control (SMC), unmanned aerial vehicle (UAV).

I. INTRODUCTION

In recent years, multirotor unmanned aerial vehicles (UAVs) have been widely developed and have become popular because of their extensive usefulness in a wide area of applications, such as military surveillance, management of natural risks, agriculture, and industrial automation. [1]. The salient advantages of multirotor UAVs are their low cost, small size, hovering capability, vertical landing and take-off capability, easy maintenance, and operation in both indoor and outdoor environments [2]. However, the design of an autonomous flight controller for indoor and outdoor quadrotors is challenging in practice due to the intrinsic under-actuation property, strong coupling between the rotational and translational dynamics, nonlinearity and external and internal disturbances such as the mass variation of payloads, gyroscopic moments and aerodynamic damping forces. In addition, it becomes more complicated when the multirotor is subjected to system faults and actuator failures [3], [4]. It is necessary to design an effective controller for tracking position and attitude to account these undesired consequences. To achieve the desired tracking performance considering the above undesired effects, several researchers have proposed various classical and adaptive control techniques, such as linear and adaptive proportional–integral–derivative (PID) controls [5], feedback linearization controls [6], backstepping control [7], sliding-mode control (SMC) [8], model predictive control (MPC) [9], adaptive controls [10]–[14], disturbance observer (DOB) [15], linear quadratic regulator (LQR) based control [16] and the recently developed intelligent control [17], [18] and event-trigger uncertainty estimator [19]–[21] for complicated systems. These controllers are demonstrated to be effective in some specific cases, but most of them are limited to the attitude-tracking problems and except for a few studies [22], [23], have received a little attention for the position-trajectory-tracking problems, which must be implemented for practical applications. Recently, research [24] has developed the robust control based on the disturbance observer (DOB) to estimate and compensate for uncertainty and delay and can be utilized

The associate editor coordinating the review of this manuscript and approving it for publication was Zhen Li.

for both the attitude and position control of quadrotor UAVs. On the other hand, many existing controllers for position- and attitude-trajectory control have paid little attention to the finite-time control and convergence to the desired trajectory under disturbance. In the existing literature, most of the finite-time control algorithms have been developed for attitude control of spacecraft, but not many have been developed for multirotor UAVs yet. Thus, they are still being investigated in the field of multirotor trajectory control in the finite-time stability and stabilization problem, which are of great theoretical and practical interest.

Finite-time control methods can be classified into two categories: homogeneous domination and Lyapunov-based approaches. Based on the homogeneous approach, a local continuous controller was designed to solve the finite-stabilization problem. However, the homogeneous domination approach cannot determine the upper-bound feature of a settling time, in particular, with model uncertainties [25]. To overcome these problems, based on the Lyapunov approach, a terminal sliding-mode control algorithm in addition to the power integrator was developed [26] and guarantees that the system converges to the equilibrium state in finite-time [27]. However, this method does not ensure fast finite-time convergence. To overcome these difficulties, a new form of nonlinear sliding manifold was proposed for formulating a fast terminal sliding-mode control (TSMC), which has the characteristic of both the linear and terminal sliding-mode controls, and has shown fast and finite-time convergence [28]. Some researchers have attempted to use the TSMC approach for the position and attitude control of a quadrotor [29]–[31]. In [29], the robust TSMC control was developed for both the fully actuated and under-actuated subsystem of the quadrotor UAV in the presence of an external disturbance. The dynamic terminal sliding-mode control (DTSMC) was extended for the finite-time position and attitude tracking for a small quadrotor UAV [30]. The finite-time control for the position and attitude of quadrotor UAV was developed [31], and the controller was compared with PD control in numerical simulation. The sliding-mode-based robust control [32] and finite-time converging control were developed and adopted in various systems in order to guarantee the stability [33]–[36]. However, most of the derivations for converging time have been proven without considering disturbance and model uncertainties. A few controllers have been developed so far for the finite-time convergence of both the attitude and position of UAVs to the sliding manifold in the presence of disturbance and model uncertainties; however, still there are limitation to UAV applications in practice. It is difficult to implement the developed TSMCs in real flight by several reasons. First, adaptive TSMC, which update gain to estimate upper bound of disturbance adaptively, was developed to eliminate steady state error without information of the upper bound [37], [38]. However, the adaptive gains will increase infinitely, because the noise will be cumulated although states are converged. Second, it often requires finding controller gain parameters by additional techniques such as system identification and gain optimization, because it is necessary to consider actuator saturation, nonlinearity, jittering and noise. In addition, there is no guideline for users to tune the controller gains, unlike classical PID control. For these reasons, there are few TSMC which implemented both attitude and position in practice, and the PID controllers are still used broadly in commercial areas. Recently, TSMC and super-twisting SMC (ST-SMC) were compared in experiments [39], but only transient response of altitude control was implemented, and guideline to find the controller gain is not still suggested clearly.

Therefore, this study focuses on designing finite-time controller, which is simple and practical to supplant PID control, in the presence of disturbances. Furthermore, properties of the controller are analysed in various simulations and experiments in order to provide a guideline for gain tuning. First, a new continuous sliding-mode control law is proposed by the finite-time control method. By construction of a suitable Lyapunov function, finite-time convergence for a tracking error to the sliding manifold is proven in the presence of disturbances. The time to reach to the sliding surface is also shown. In order to show the robustness of the proposed controller, a disturbance torque model due to misalignment between the centre of mass and centre of rotation of the multirotor system and wind disturbances are considered in the UAV dynamics. In addition, the method enables tuning of the gain parameters of the finite-time sliding-mode controls corresponding to a conventional PID controller. Thus, the gain parameters of the finite time sliding-mode controller can be similarly computed by the PID controller. This reduces the computational burden to determine the properly tuned control gains. Finally, the designed controller and gain parameters are experimentally applied and verified. The characteristics of the controller according to various gain parameters is shown, and the robustness and tracking performance are compared with the PID controller and recent adaptive sliding mode control (ASMC) [37]. The paper is organized as follows. In Section II, preliminaries on multirotor dynamics and kinematics are briefly presented. In Section III, the finite-time controls for the position and attitude to their desired states, followed by the finite-time stability to the sliding manifold, are presented. Section IV provides a guide to find the proper control gain. Numerical simulations and experiments for regulation and tracking controls are compared to show the robustness and effectiveness of the proposed work. Finally, Section V presents the concluding remarks on this research.

II. SYSTEM DEFINITION

Fig. 1 shows the conceptual design of a multirotor UAV. The UAV could have a number of actuators and rotors, but it is an under-actuated system because it could have the maximum four-rank input matrix for controlling six degrees of freedom, regardless of the number of inputs. In other words, the attitude of roll and pitch motions are coupled to the position.

For simplicity, the multirotor is considered to be a symmetric rigid body and the motion of the multirotor is described by

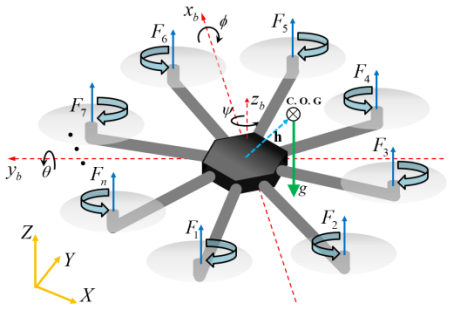

FIGURE 1. Schematic of a multirotor UAV.

Euler's equation. Two frames, the inertial and body frames, are considered for the mathematical formulations of the multirotor dynamics. The origin of the body frame (x_b-y_b-z_b) coincides with the centre of rotation of the multirotor and the axes are aligned along the principle moments of inertia. The position of the multirotor in the inertial reference frame is denoted by the vector (x,y,z) and the orientation of multirotor that referred to by the roll, pitch, and yaw (ϕ, θ, ψ), which are measured from the inertial frame of reference.

The dynamics of the multirotor are expressed as

$$\dot{\mathbf{X}} = f(\mathbf{X}) + g(\mathbf{X})\mathbf{U}, \tag{1}$$

where the state variable $\mathbf{X} = [x\ y\ z\ \phi\ \theta\ \psi\ \dot{x}\ \dot{y}\ \dot{z}\ \dot{\phi}\ \dot{\theta}\ \dot{\psi}] = [x_1\ x_2 \ldots x_{12}]$;

$$\begin{aligned}
\dot{x}_i &= x_{i+6} \quad \text{for } i = 1, 2, \ldots, 6 \\
\dot{x}_7 &= u_x - K_1 x_7 + \sigma_1 \\
\dot{x}_8 &= u_y - K_2 x_8 + \sigma_2 \\
\dot{x}_9 &= u_z - K_3 x_9 + \sigma_3 \\
\dot{x}_{10} &= U_2 - \frac{I_r x_{11}\Omega}{I_{xx}} - K_4 x_{10} + G_\phi + \zeta_4 \\
\dot{x}_{11} &= U_3 + \frac{I_r x_{10}\Omega}{I_{yy}} - K_5 x_{11} + G_\theta + \zeta_5 \\
\dot{x}_{12} &= U_4 - K_6 x_{12} + G_\psi + \zeta_6,
\end{aligned} \tag{2}$$

$$\begin{aligned}
u_x &= (\cos(x_4)\sin(x_5)\cos(x_6) + \sin(x_6)\sin(x_4))U_1 \\
u_y &= (\cos(x_4)\sin(x_5)\sin(x_6) - \sin(x_4)\cos(x_6))U_1 \\
u_z &= \cos(x_4)\cos(x_5)U_1 - g
\end{aligned} \tag{2a}$$

where U_1, U_2, U_3, and U_4 are the thrust forces in (3a) and (3b) as the position and attitude system inputs; $K_i (i = 1, 2, \ldots, 6)$ is the aerodynamic drag coefficient; G_ϕ, G_θ, and G_ψ are torque vectors due to the centre of gravity detailed in (3c); $\sigma_i (i = 1, 2, 3)$ represents the wind disturbances in position control; u_x, u_y, and u_z are the virtual control in (2a); and ζ_i $(i = 4, 5, 6)$ is the torque caused by the gyroscopic effect and given in (3d); Ω indicates effect of the propellers on the angular moments; g is gravitational acceleration; I_r is the moment of inertia of the rotors; I_{xx}, I_{yy}, and I_{zz} in (2a) and (3a) are the principal moments of inertia of a multirotor UAV along the x_b, y_b, and z_b axes respectively.

$$\begin{bmatrix} U_1 \\ U_2 \\ U_3 \\ U_4 \end{bmatrix} = \mathbf{\Lambda F} = \begin{bmatrix} 1/m & 1/m & \cdots & 1/m \\ l_{1x}/I_{xx} & l_{2x}/I_{xx} & \cdots & l_{nx}/I_{xx} \\ l_{1y}/I_{yy} & l_{2y}/I_{yy} & \cdots & l_{ny}/I_{yy} \\ c_1/I_{zz} & c_2/I_{zz} & \cdots & c_n/I_{zz} \end{bmatrix} \times \begin{bmatrix} F_1 \\ F_2 \\ \vdots \\ F_n \end{bmatrix}, \tag{3a}$$

$$\mathbf{F} = \mathbf{\Lambda}^T \left(\mathbf{\Lambda}\mathbf{\Lambda}^T\right)^{-1} \mathbf{U}, \tag{3b}$$

$$\begin{bmatrix} I_{xx}G_\phi \\ I_{yy}G_\theta \\ I_{zz}G_\psi \end{bmatrix} = \begin{bmatrix} h_x \\ h_y \\ h_z \end{bmatrix} \times m\mathbf{R}^T \begin{bmatrix} 0 \\ 0 \\ -g \end{bmatrix}, \tag{3c}$$

$$\begin{aligned}
\zeta_4 &= (I_{yy} - I_{zz})x_{11}x_{12}/I_{xx} \\
\zeta_5 &= (I_{zz} - I_{zz})x_{10}x_{12}/I_{yy} \\
\zeta_6 &= (I_{xx} - I_{yy})x_{10}x_{11}/I_{zz}
\end{aligned} \tag{3d}$$

where constants l_{ix}, l_{iy}, and c_i $(i = 1, 2, \ldots, n)$ are the x and y components of the length from the centre of the UAV to the i^{th} motor and the coefficients that generate torque in the yaw angle ψ, respectively with n motors; F_i $(i = 1, 2, \ldots, n)$ is thrust force generated by i^{th} motor. The desired motor input $\mathbf{F}$ can be obtained with optimization with 2-norm in (3b) with the assumption that the rank of $\mathbf{\Lambda}$ is larger than 4 where $\mathbf{U}$ is a control output defined by $\mathbf{U} = [U_1,\ U_2,\ U_3,\ U_4]$. $\mathbf{h} = [h_x,\ h_y,\ h_z]^T$ is the distance vector from the centre of rotation to the centre of mass with respect to the body frame. $\mathbf{R}$ is the rotation matrix from the body to the inertial frame.

III. FINITE-TIME TRACKING CONTROLLER

A finite-time tracking controller based on a nonlinear sliding-mode control is developed for the performance of both position and attitude. The nonlinear sliding manifolds and nonlinear reaching laws, which alleviate chattering, are designed first. The virtual control will be derived based on the sliding manifolds and reaching laws, in turn, used to derive desired roll and pitch angles, and thrust for position control. Then, the stability of the control algorithm will be derived based on the sliding surfaces and nonlinear reaching laws.

A. FINITE-TIME POSITION-TRACKING CONTROLLER

Finite-time virtual control is designed and followed by global asymptotic stability in Proposition 1. The finite-time reachability of equilibrium points to the origin of the sliding surfaces is shown in order to follow the desired position trajectory (x_{1d}, x_{2d}, x_{3d}).

Proposition 1: Let us consider the continuous differentiable sliding manifold for the position tracking and a standard state-feedback power rate reaching law for the control, chosen as (4) and (5), respectively.

$$s_i = \dot{\varepsilon}_i + a_i p(\varepsilon_i), \tag{4}$$

$$\begin{cases} p(\varepsilon_i) = |\varepsilon_i|^{b_i} \operatorname{sgn}(\varepsilon_i), & \text{if } |\varepsilon_i| \geq B_i \\ p(\varepsilon_i) = \dfrac{B_i^{b_i-3}}{2}\left[(b_i-1)\,\varepsilon_i^3 + (3-b_i)\,B_i^2\varepsilon_i\right], & \text{if } |\varepsilon_i| < B_i \end{cases} \tag{4a}$$

$$\begin{cases} p'(\varepsilon_i) = b_i\,|\varepsilon_i|^{b_i-1}, & \text{if } |\varepsilon_i| \geq B_i \\ p'(\varepsilon_i) = \dfrac{B_i^{b_i-3}}{2}\left[3\,(b_i-1)\,\varepsilon_i^2 + (3-b_i)\,B_i^2\right], & \text{if } |\varepsilon_i| < B_i \end{cases} \tag{4b}$$

where $dp(\varepsilon_i)/d\varepsilon_i = p'(\varepsilon_i)$

$$\begin{aligned} \dot{s}_i &= (-d_i\,|s_i|^{e_i}\,sgn(s_i) - c_i\int s_i dt)/(1+K_{di}) \\ &= -d_i\,|s_i|^{e_i}\,sgn(s_i) - c_i\int s_i dt - K_{di}\dot{s}_i \end{aligned} \tag{5}$$

with positive constants a_i, b_i, c_i, d_i, e_i, and K_{di} ($i = 1, 2, 3$ corresponding to x, y, z, respectively), and ε_i is an error defined as $\varepsilon_i = x_{id}$-x_i where $i = 1, 2, \ldots, 6$ for all the states including position and attitude in (2). B_i in (4a) can be chosen as small enough to avoid singularity when $0 < b_i < 1$ and $\varepsilon_i = 0$. In addition, it can be set as $B_i = 0$ if $b_i \geq 1$. Then, virtual controls u_1, u_2, and u_3 corresponding to u_x, u_y, and u_z for position tracking can be expressed as (6).

$$\begin{aligned} u_i = \ddot{x}_{id} + K_i\dot{x}_i + a_i p'(\varepsilon_i)(\dot{x}_{id} - \dot{x}_i) \\ + d_i\,|s_i|^{e_i}\,sgn(s_i) + c_i\int s_i dt + K_{Di}\dot{s}_i \end{aligned} \tag{6}$$

Proof: The time derivative of the sliding variables in (4) along the trajectories of the closed-loop system is given by (7).

$$\begin{aligned} \dot{s}_i &= \ddot{\varepsilon}_i + a_i p'(\varepsilon_i)\dot{\varepsilon}_i \\ &= \ddot{x}_{id} - u_i + K_i\dot{x}_i - \sigma_i + a_i p'(\varepsilon_i)(\dot{x}_{id} - \dot{x}_i) \end{aligned} \tag{7}$$

From (5) and (7), the respective controls for the position tracking can be presented as (6) except disturbance σ_i. Furthermore, the stability of the sliding manifold must be satisfied to ensure the stability of the control system. In Proposition 2, the finite-time stability and the time to reach the sliding manifold can be proven.

Proposition 2: Consider that the kinematics of the UAV in (2) and the proposed control law given by (6) makes the trajectory of the UAV to converge to the desired trajectory in finite time and stays in the sliding manifold.

Proof: Let the Lyapunov candidate function be defined by a radially unbounded positive-definite function as

$$V_i = \frac{1}{2}\left[(1+K_{Di})s_i^2 + c_i\left(\int s_i\,dt + \sigma_i/c_i\right)^2\right], \tag{8}$$

where $i = 1, 2, 3$. The time derivative of (8) can be simplified as (9).

$$\begin{aligned} \dot{V}_i &= s_i\left((1+K_{Di})\dot{s}_i + c_i\int s_i dt + \sigma_i\right) + \dot{\sigma}_i\left(c_i\int s_i\,dt + \sigma_i\right) \\ &= s_i\left(K_{Di}\dot{s}_i + \dot{s}_i + c_i\int s_i dt + \sigma_i\right) + \dot{\sigma}_i\left(c_i\int s_i\,dt + \sigma_i\right) \\ &= s_i\left(K_{Di}\dot{s}_i + \ddot{x}_{id} - u_j + K_i\dot{x}_i - \sigma_i + a_i p'(\varepsilon_i)\dot{\varepsilon}_i \ldots\right. \\ &\quad \left. + c_i\int s_i dt + \sigma_i\right) + \dot{\sigma}_i\left(c_i\int s_i\,dt + \sigma_i\right) \\ &= s_i\left(K_{Di}\dot{s}_i + \ddot{x}_{id} - \ddot{x}_{id} - K_i\dot{x}_i - a_i p'(\varepsilon_i)\dot{\varepsilon}_i\right. \\ &\quad - d_i\,|s_i|^{e_i}\,sgn(s_i) - c_i\int s_i dt - K_{Di}\dot{s}_i - \sigma_i \\ &\quad \left. + K_i\dot{x}_i + a_i p'(\varepsilon_i)\dot{\varepsilon}_i + c_i\int s_i dt + \sigma_i\right) + \dot{\sigma}_i\left(c_i\int s_i\,dt + \sigma_i\right) \\ &= s_i(-d_i\,|s_i|^{e_i}\,sgn(s_i)) + \dot{\sigma}_i\left(c_i\int s_i\,dt + \sigma_i\right) \\ &\leq -d_i\,|s_i|^{e_i+1} + |\dot{\sigma}_i|\left(c_i\int s_i\,dt + \sigma_i\right) = -d_i\,|s_i|^{e_i+1} \\ &\leq 0 \end{aligned} \tag{9}$$

The convergence of s_i to 0 can be proven as (9) with assumption that the disturbance varies slowly enough to assume $|\dot{\sigma}_i| \approx 0$. Convergence of $\left|\int s_i\,dt + \sigma_i/c_i\right|$ to 0 when s_i converges to 0 is also guaranteed by (6) and (7). Therefore, it can be said that the convergence of V_i is guaranteed when s_i converges to 0.

Lyapunov stability is ensured in the presence of a disturbance. The finite-time convergence of the attitude states to the origin of the sliding manifold takes place, as shown in the following. Before deriving the expression for convergence time, the following definition and lemmas must be considered.

Definition 3: Consider a time-invariant system represented by a differential equation given in (10).

$$\dot{z} = f(z) \tag{10}$$

where $f\colon D \to R^{\mathrm{n}}$ is continuous on an open neighbourhood D of the origin and $f(0) = 0$, $y \in R^{\mathrm{n}}$ and $y(0) = y_0$. The zero solution of the system in (10) is (locally) finite-time stable if it is Lyapunov stable and finite-time convergent in open neighbourhood $U \subseteq D$. $U = D = R^n$. Here, the finite-time convergence implies that for any initial condition $y_0 \in U\backslash\{0\} \to (0, \infty)$, every solution $y(t, y_0)$ of the system in (10) is defined with $y(t, y_0) \in U\backslash\{0\}$ for $t \in [0, T_{y(0)}]$ and satisfies $\lim_{t\to T(y)} y(t, y_0) = 0$, and $y(t, y_0) = 0$ if $t \geq T(y_0)$ [27].

Lemma 4: Consider the system described by (10). Suppose there is a continuously differentiable (C^1) scalar function V defined in open neighbourhood $D \subset R^{\mathrm{n}}$ of the origin and there are real numbers $m_0 > 0$ and $0 < n_0 < 1$ such that V is positive definite on D and satisfies the condition on D.

$$\dot{V}(y) + m_0 V^{n_0}(y) \leq 0 \tag{11}$$

Then, the origin of the system in (8) for a given initial condition $y(0) = y_0$ (some open neighbourhood of the origin) is locally finite-time stable and the convergence time T_{y_0} satisfies condition (12).

$$T_{y_0} \leq \frac{1}{m_0(1-n_0)} V(y_0)^{1-n_0} \tag{12}$$

Moreover, for $D = R^n$, if V is radially unbounded, then the origin is globally finite-time stable [27].

Now, let us define the positive constant δ as $\delta \geq \left|\int s_i\,dt + \sigma_i/c_i\right|$, and (9) can be rewritten as

$$\dot{V}_i = -d_i\,|s_i|^{(1+e_i)} \leq -d_i \cdot \left|(2V_i - c_i\delta^2)/(1+K_{di})\right|^{(1+e_i)/2}. \tag{13}$$

As the Lyapunov function is radially unbounded, the closed-loop position-control system in (7) with the control law in (6) is globally stable. Moreover, for the given initial conditions of the sliding variables, the time to reach the origin of the sliding manifold can be derived based on Lemma 4 and the definitions. Let $s_{i,0}$ be the initial condition of the sliding surface for the corresponding initial values $x_i(0)$. According to Lemma 4, the settling time to reach the origin of the sliding manifold $s_i = 0$ can be derived for the two cases. The convergence time for the two cases when $V_{s_{i,0}} < c_i\delta^2/2$ and $V_{s_{i,0}} \geq c_i\delta^2/2$ can be derived as (14) and (15), respectively.

$$T_{s_{i,0}} \leq \frac{(1+K_{di})^{(e_i+1)/2}}{d_i(1-e)\cdot 2^{(e_i-1)/2}} \cdot \left((\frac{c_i\delta^2}{2})^{(1-e_i)/2} - (\frac{c_i\delta^2}{2} - V_{s_{i,0}})^{(1-e_i)/2}\right) \tag{14}$$

$$T_{s_{i,0}} \leq \begin{cases} \dfrac{(1+K_{di})^{(e_i+1)/2}}{d_i(1-e)\cdot 2^{(e_i-1)/2}} \left((V_{s_{i,0}} - \frac{c_i\delta^2}{2})^{(1-e_i)/2} + (\frac{c_i\delta^2}{2})^{(1-e_i)/2}\right) & : 0 < e_i < 1 \\ \infty & : 1 \leq e_i \end{cases} \tag{15}$$

Equations (14) and (15) ensure that the trajectory of the system reaches the sliding manifold $s_i = 0$ within the finite time $T_{s_{i,0}}$ with $0 < e_i < 1$.

Remark 5: It is difficult to control all states independently because the rank of input matrix $\mathbf{\Lambda}$ is 4. For this reason, the desired ϕ_d, θ_d, and total thrust U_1 will be chosen to generate virtual controls u_x, u_y, and u_z in order to track the desired position. From (2a), U_1, ϕ_d, and θ_d can be obtained as in (16) and (17). The desired yaw angle, x_{6d}, is used instead of x_6 by assuming rapid convergence of x_{11} to x_{11d}.

$$U_1 = \sqrt{\left(u_x^2 + u_y^2 + (u_z^2 + g)^2\right)} \tag{16}$$

$$\begin{cases} x_{4d} = \sin^{-1}\left(\left(u_x \sin x_{6d} - u_y \cos x_{6d}\right)\dfrac{1}{U_1}\right) \\ x_{5d} = \tan^{-1}\left(\dfrac{u_x \cos x_{6d} + u_y \sin x_{6d}}{u_z + g}\right) \end{cases} \tag{17}$$

B. FINITE-TIME ATTITUDE-TRACKING CONTROLLER

The finite-time control for tracking the attitude is developed similarly to that for the position control. The desired ϕ and θ will be used for deriving the errors between the reference and current attitudes. The attitude control is derived for attitude tracking based on the same procedure as in the position control. Control output of attitude control can be obtained as (18) based on (4) and (5).

$$U_{i-2} = \ddot{x}_{id} - \zeta_i + K_i\dot{x}_i + a_i p'(\varepsilon_i)(\dot{x}_{id} - \dot{x}_i) + d_i\,|s_i|^{e_i}\,\mathrm{sgn}(s_i) + c_i\int s_i dt + K_{Di}\dot{s}_i \tag{18}$$

where $i = 4$, 5, and 6, corresponding to ϕ, θ, and ψ, respectively.

Proposition 6: Consider the dynamics of the UAV in (2) and the proposed control law given by (18), then there exist a_i, b_i, c_i, d_i, and e_i ($i = 4, 5, 6$) such that the control laws in (18) make the state of (2) converge to the desired state in finite time and remain in the sliding manifold.

Proof: To reduce repetition, the stability analysis of the roll angle is shown only for ϕ_d, $\theta_d = 0$ but can be applied for tracking the pitch and yaw motion trajectories. Let the Lyapunov function be defined by a radially unbounded positive-definite function in (19).

$$V_\phi = \frac{1}{2}\left[(1+K_{D\phi})s_\phi^2 + c_\phi\left(\int s_\phi\,dt - \frac{mgh_y}{c_\phi I_{xx}}\right)^2\right] \tag{19}$$

The time derivative of the above energy functions with the unknown G_ϕ of (2) manifests

$$\begin{aligned} \dot{V}_\phi &= s_\phi\left((1+K_{D\phi})\dot{s}_\phi + c_\phi\int s_\phi\,dt - \frac{mgh_y}{I_{xx}}\right) \\ &= -d_\phi\,|s_\phi|^{e_\phi+1} - s_\phi(\frac{mgh_z}{I_{xx}}\cdot\sin\phi\cos\theta - \frac{mgh_y}{I_{xx}} \\ &\quad \cdot\cos\phi\cos\theta + \frac{mgh_y}{I_{xx}}) \\ &\leq -d_\phi|s_\phi|^{e_\phi+1} + |s_\phi|\left(\sqrt{\left(\frac{mgh_z}{I_{xx}}\right)^2 + \left(\frac{mgh_y}{I_{xx}}\right)^2} + \frac{mgh_y}{I_{xx}}\right) \\ &< 0, \end{aligned} \tag{20}$$

The inequality of (20) is satisfied when the following condition holds.

$$|s_\phi| > \left((\sqrt{\left(\frac{mgh_z}{I_{xx}}\right)^2 + \left(\frac{mgh_y}{I_{xx}}\right)^2} + \frac{mgh_y}{I_{xx}})/d_\phi\right)^{1/e_\phi} \tag{21}$$

In (21), the sufficiently large gain parameter d_ϕ and $0 < e_\phi < 1$ can make ϕ approach 0. This in turn makes $\sin\phi \approx 0$, $\cos\phi \approx 1$. Furthermore, it is assumed that θ is converged to 0 and $\cos\theta \approx 1$ for the decoupled motion. Considering these conditions, (20) becomes

$$\begin{aligned} \dot{V}_\phi &= s_\phi\left((1+K_{D\phi})\dot{s}_\phi + c_\phi\int s_\phi\,dt - \frac{mgh_y}{I_{xx}}\right) \\ &= -d_\phi\,|s_\phi|^{e_\phi+1} \prec 0 \end{aligned} \tag{22}$$

This ensures that $\dot{V}_\phi < 0$ except at the origin, implying that $s_\phi \to 0$ under the control law in (18). The finite-time stability of the attitude control also can be proven in a similar way as the position control. Near an equilibrium point, (22) can be written as in (23) with the positive constant δ as $\delta \geq \left|\int s_\phi\,dt - \frac{mgh_y}{c_\phi I_{xx}}\right|$.

$$\begin{aligned} \dot{V}_\phi &= -d_\phi\,|s_\phi|^{e_\phi+1} \\ &\leq -d_\phi \cdot \left|(2V_\phi - c_\phi\delta^2)/(1+K_{D\phi})\right|^{(e_\phi+1)/2} \end{aligned} \tag{23}$$

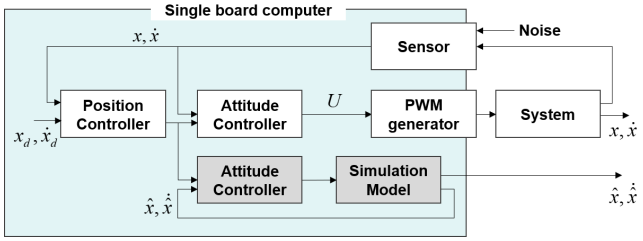

FIGURE 2. Block diagram of experimental system.

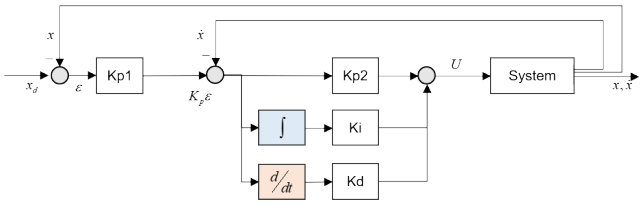

FIGURE 3. Control block diagram of a PID controller.

TABLE 1. Experimental hardware setup and system parameters.

		Controller	Raspberry pi 3
		IMU sensor	MPU 9250
		Motor	2212/920 kV
		Battery	Li-Po 11.1 V 3000 mAh
		Weight, m	1.2 kg
		Diameter	550 mm
L/I_{xx}, L/I_{yy}	5.07 m·rad/Ns^2	mgh_z/I_{xx}	12.28 m·rad/s^2
C/I_{zz}	2.34 rad/Ns^2	mgh_y/I_{xx}	-0.35 m·rad/s^2
K_ϕ, K_θ, K_ψ	≈ 0	mgh_z/I_{yy}	12.56 m·rad/s^2
F_1, F_2, F_3, F_4	0–5.4 N	mgh_x/I_{yy}	-0.16 m·rad/s^2

Now, for the given initial conditions of the sliding variables, the time to reach the sliding manifold can be derived based on the same procedures as the finite-time reachability of the position. Let $s_{\phi,0}$ be the initial condition of the sliding surface for the corresponding initial values of roll $x_\phi(0)$. According to Lemma 4, the convergence time to reach the origin of the sliding manifold $s_\phi = 0$ can be written the same as (14) and (15). This ensures that $s_\phi \to 0$ in finite time, which can be achieved for $0 < e_\phi < 1$.

IV. RESULTS AND DISCUSSION

Both numerical and experimental results on a quadrotor UAV are demonstrated in the presence of modelled uncertainty and disturbance to show robustness of the controller. For the uncertainty, the difference between the centre of rotation and gravity is considered in attitude control. The wind disturbance is injected in the position control experiment. The experimental composition and physical parameters of the UAV are summarized in Table 1. Fig. 2 shows a control system consisting of the UAV and hardware-in-the-loop simulations (HILS) for the experimental analysis. The attitude and angular velocities of the UAV are measured by an inertial measurement unit (IMU) sensor, and the attitude control loop was operated at 200 Hz. The position and velocity are measured by a motion-capture system and the position control is operated at 120 Hz. Before the flight experiments, parameters in Table 1 are identified and verified by comparing the physical hardware and model output in parallel with the HILS, as described in Fig. 2. In addition, the control algorithm and gain parameters are verified by numerical simulation. The simulations and experiments are implemented in two ways. First, the effect of the change in the nonlinear parameter e in (18), which is power index of s, will be shown. Second, the attitude regulation and tracking performance of the quadrotor UAV with the high centre of mass are compared to those of a conventional PID controller. The position regulation under wind disturbance and tracking performance are compared by experiments.

A. CONTROL GAIN PARAMETER RENAMING

It is difficult in practice to understand and determine the effect of controller gains, as there are numerous control parameters in the finite-time control laws. The gain parameters of the finite-time controller are renamed below by comparing their roles with that of the parameters of the widely used classical PID controller in order to provide a guide to tune the gain parameters. The PID controller shown in Fig. 3 can be written as

$$U = (K_{P1}K_{P2} + K_I)\varepsilon + (K_{P1}K_D + K_{P2})\dot{\varepsilon} + K_D\ddot{\varepsilon} + K_{P1}K_I \int \varepsilon \, dt \tag{24}$$

where K_{P1}, K_{P2}, K_I, and K_D are gain parameters of the PID controller in Fig. 3.

It is assumed that the gyroscopic force and drag are negligible and gain parameters b and e are set as 1 in (18) to compare both controllers. Similarly, the finite-time controller can be expressed along with the PID gain parameters as in (25), and the corresponding block diagram is shown in Fig. 4.

$$\begin{aligned} U &= (ad + c)\varepsilon + (a + d + aK_D)\dot{\varepsilon} + K_D\ddot{\varepsilon} + ac \int \varepsilon \, dt \\ &= (K_{P1}K_{P2} + K_I)\varepsilon + (K_{P1} + K_{P2} + K_{P1}K_D)\dot{\varepsilon} \\ &\quad + K_D\ddot{\varepsilon} + K_{P1}K_I \int \varepsilon \, dt \end{aligned} \tag{25}$$

where the control gains indicate $K_{P1} = a$, $K_{P2} = d$, and $K_I = c$. b and e in (18) are also renamed as α and β respectively.

B. CONTROL GAIN TUNING & SIMULATION

The controller gains of both PID and finite-time controllers are optimized to achieve performance in the transient response, maximum overshoot and settling time. The gains are initially based on the dynamic model of the identified quadrotor system in (2) and Table 1. First, the gyroscopic moment of (2) is regarded as the unknown and neglected for

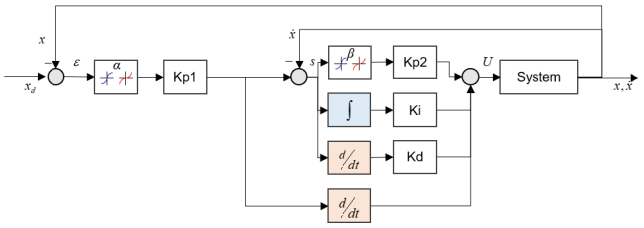

FIGURE 4. Control block diagram of a finite-time controller.

TABLE 2. Control gain sets.

Controller		K_{P1}	α	K_{P2}	K_I	K_D	β
Attitude	PID	3	-	9.5	3.7	0	-
	F-time	6	1	10	0.5	0.2	0.9
Position	PID	0.8	-	4	0.1	0.4	-
	F-time	0.8	0.8	4	0.1	0.4	0.7

TABLE 3. Performance comparison without uncertainty.

Control	Attitude (ϕ)		Position (x)	
	PID	F-time	PID	F-time
t_s (s)	0.78	0.8	3.8	3.6
OS (%)	0	0.37	0	0

t_s: settling time; OS: maximum overshoot

the decoupled dynamics. The disturbances σ_i $(i = 1, 2, 3)$, G_ϕ, G_θ, and G_ψ are also regarded as unknown disturbances and uncertainties. Initially, they are neglected for parameter identification and control optimization. Second, the transfer function of the multirotor attitude dynamics decoupled from each orientation is applied as a plant model in Matlab. Gain parameters of the PID control are optimized for the robust response of the plant and target settling time. Finally, the procedure to obtain gain parameters of the attitude control is repeated for the position control. Gain parameters of the finite-time control and ASMC are selected to achieve the same transient response as PID in the numerical simulation to compare the robustness against disturbance. Especially in position control, gain parameters of finite-time control are selected to be the same as those of PID, but only α and β are modified to obtain the transient response. The gain parameters of both controllers are obtained as shown in Table 2, and the results of the transient response, settling time and maximum overshoot, in the numerical simulation are described in Table 3 and Fig. 5.

The settling time of both orientation and position are computed as shown in Fig. 5(a) and (b) respectively. The convergence times to sliding manifolds are marked in Fig. 5(c) and (d) as c.time. The convergence time of the finite-time control are calculated to 1.3 and 0.9 seconds by (15) for the attitude and position respectively. It is assumed that integral action is converged fast and δ is assumed to be 0. s_x is converged to 0 before the precalculated convergence time in Fig. 5(d), although the position is not converged yet. Fig. 6(a) and (b) show the roll angle and control output of each controller when variances of measurement noise are 5×10^{-4} and 0.22 for

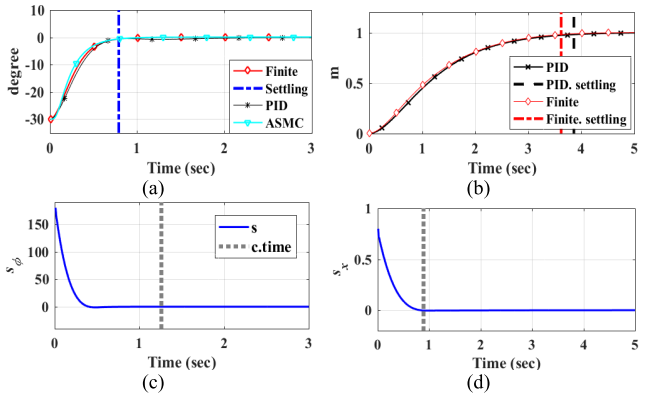

FIGURE 5. Transient response of controllers after tuning. (a) Attitude, (b) Position, (c) s_ϕ, (d) s_x.

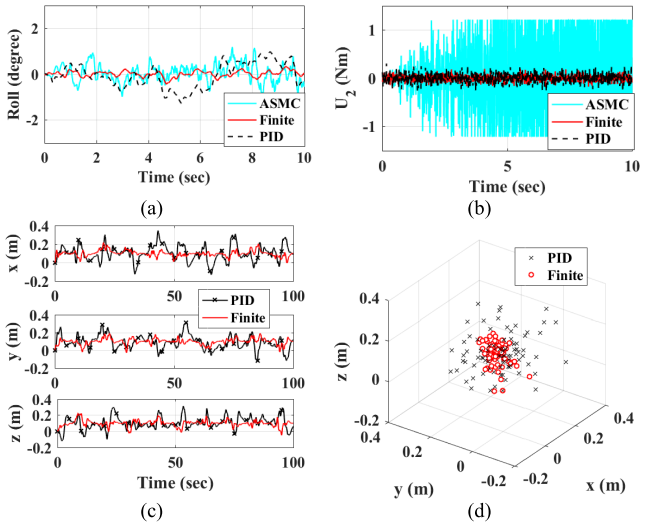

FIGURE 6. Comparison of regulation under noise and disturbance. (a) roll angle, (b) control output, (c) x, y, z positions, (d) position in 3D space.

the roll angle and angular rate respectively. RMS of control output U_2 in Fig. 6(b) are 0.065, 0.096 and 1.17 Nm for the finite-time control, PID and ASMC respectively. Magnitude of U_2 of ASMC in Fig. 6(b) increases and exceed the control limit 1.2 Nm. The reason is that adaptive gain increase without convergence because adaptation law is a positive function and noise is cumulated. For the reason, it could be difficult to apply ASMC to the flight controller with low-cost sensors, although it rejects disturbance well [37]. Fig. 6(c) and (d) show the position of the UAV and variance in the position with random disturbance bounded by the maximum of 12 N to simulate windy weather. The mean error of the finite-time control is 0.04 m and the error of the PID control is 0.11 m, twice that of finite-time control. It was shown that the finite-time control can control the system in a more robust manner.

C. EXPERIMENTAL RESULTS IN ATTITUDE CONTROL

The simulations and experiments are implemented for analysing (i) effect of the exponential gain parameter β in regulation and comparing (ii) regulation and (iii) tracking performance with disturbance and uncertainty to be compared

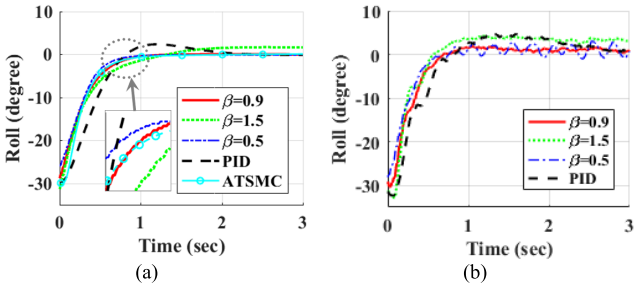

FIGURE 7. Transient response of controllers with model uncertainty. (a) Numerical simulation, (b) Experiment.

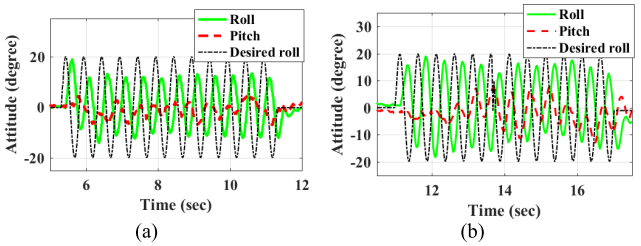

FIGURE 8. Experimental results of attitude-tracking control with 2-Hz trajectory. (a) Finite-time control, (b) PID control.

TABLE 4. Experimental performance comparison.

Controller	Attitude		Position	
	Response (overshoot) (%)	Tracking (phase delay) (rad)	Regulation (error) (m)	Tracking (error) (m)
F-time	7	2.05	0.072	0.11
PID	15.9	2.92	0.197	0.24

with the PID controller. The initial attitude is $[-30°\ 0\ 0]$ and desired attitude $[0\ 0\ 0]$ to compare the regulation performance of roll control when the centre of mass of the UAV is far from the centre of rotation. The uncertainty due to the centre of mass was identified and reflected in the simulation of Fig. 7. The control gain parameters of both controllers are same as in Table 2, but parameter β in (25) is chosen with three different values 0.9, 1.5, and 0.5 to show the effects of the nonlinear term in the controller on performance. The attitude control in Fig. 7(a) is simulated under model uncertainty due to misaligned centre of mass, G_ϕ, G_θ, and G_ψ in (2). The settling time of the PID control and ASMC increased from 0.78 to 1.93 s (147%) and 0.78 s to 1.01 s (29%) respectively, whereas the finite-time control ($\beta = 0.9$) increased from 0.8 to 0.93 s (16%). The maximum overshoot increased to 7.9%, 1.1% and 1.67% in the PID, ASMC and finite-time control results, respectively comparing to Fig. 5(a) without uncertainty.

The orientation response converges quickly with a smaller β parameter ($\beta = 0.5$). However due to the characteristic of the function with order less than 1, the controller becomes more sensitive to sensor noise near the equilibrium so data with $\beta = 0.5$ in Fig. 7 (b) fluctuates with a large amplitude when the sensor noise is amplified. The response is smooth with a larger β parameter ($\beta = 1.5$), but the convergence is slow, and the converging time cannot be assured due to (15). Therefore, it is important to choose proper α and β values for better performance. The further results and description of the finite-time control in attitude use the gain set $\beta = 0.9$, as described in Table 2. The 'c.time' in Fig. 7 is the converging time of the controller with $\beta = 0.9$, as calculated by (15). The states converged to a sliding surface before the calculated finite time, and the roll angle also settled to the equilibrium point.

In good flying conditions without disturbance and model uncertainty, the PID controller performed as good as the finite-time controller, as shown in Fig. 5. The performance is mainly dependent on the controller gain parameters. However, the transient response of the PID controller in Fig. 7 became worse in both the simulation and experiment due to model uncertainty. In the experiment, overshoot and settling time of the PID control are 15.9% and 2.6 s, respectively, but only 7% and 0.7 s in the finite-time control result for $\beta = 0.9$. Although the transient response in the ideal model were the same as in Table 3, the results demonstrate the robustness of the finite-time control. Furthermore, the sliding surface of the finite-time controller can be designed, and the response will converge in finite time and slide on the surface.

The experiments are implemented with a desired roll angle trajectory of a 2Hz sinusoidal function in order to show the tracking performance. Both desired angles of the pitch and yaw are set to zero. The experimental results of the attitude-tracking control with 2-Hz desired trajectory are shown in Fig. 8. There is large disturbance in the pitch angle when the roll angle moves fast because the dynamics of roll and pitch angle are coupled. In that case, it is shown that the designed controller is more stable in the roll motion and regulates pitch motion better, whereas the result of the PID controller is almost out of phase (i.e., cannot be followed). The average phase delay of the finite-time control and PID are 2.05 and 2.92 rad, respectively. The parameter β contributes to better performance, and the controller is designed to reach and follow the sliding surface.

D. EXPERIMENTAL RESULTS IN POSITION CONTROL

The performance of the position control is compared with the PID controller in experiments. The gain sets of Table 3 are used for both controllers in the position and attitude. The same control and gain parameters are used for the attitude control to compare only the position-control performance. First, the regulation performance is demonstrated with the wind disturbance, and the results are shown in Fig. 9.

As shown in the result, the proposed controller regulates position robustly with gust (5 m/s) as a disturbance. The effects of α and β in (6) make the system more robust near the equilibrium state. The average position error of the finite-time control and PID control were 0.072 m and 0.197 m, respectively.

The tracking experiments were implemented with a circular trajectory. The radius of the trajectory was 0.5 m and frequency of the trajectory was 0.33 Hz. The finite-time

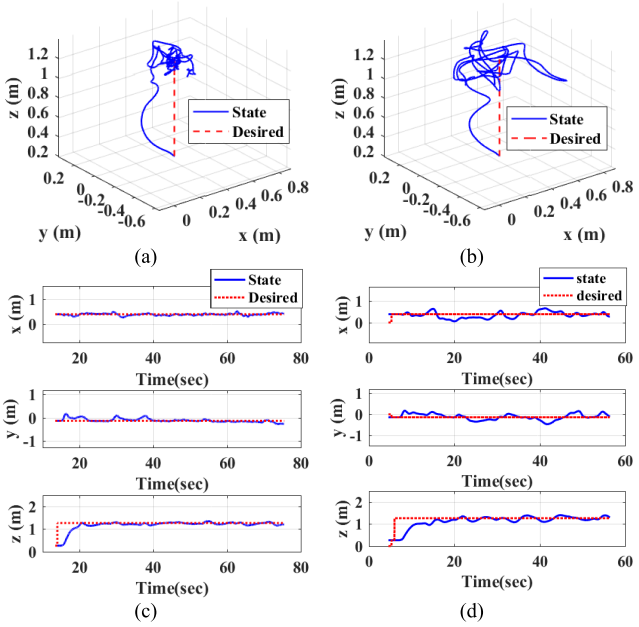

FIGURE 9. Experimental results under wind disturbance. (a) Finite-time control in 3-D space, (b) PID control in 3-D space, (c) Finite-time control in time domain, (d) PID control in time domain.

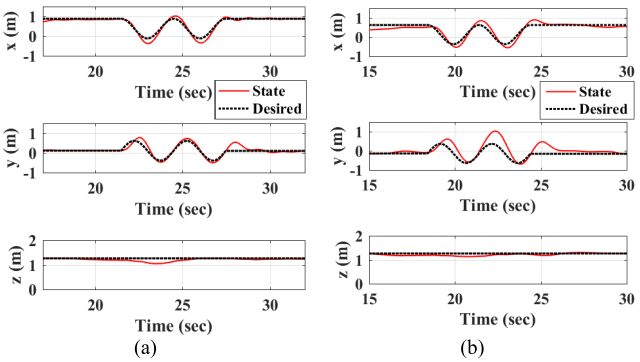

FIGURE 10. Experiments on position-tracking control. (a) Finite-time control, (b) PID control.

controller tracked the position of the sinusoidal trajectory with a small error and phase delay compared to those of the PID controller. The average position error of the finite-time control was 0.11 m, whereas that of the PID control was 0.24 m. This shows that the finite-time control can be applied to track the trajectory of a higher frequency.

V. CONCLUSION

In this paper, a new finite-time control for multirotor UAVs with disturbance has been developed. First, the finite-time control was designed for position tracking to the desired trajectory, which is in turn used to find the desired roll and pitch angles. It has been proven that the position of the multirotor reaches the desired trajectory in finite-time. Similar to the position control, the finite-time control laws have been developed for attitude. The finite-time stability was proven with a Lyapunov-like function, including an integral in the existence of disturbance. The stability and control performance for both regulation and tracking is illustrated using a quadcopter UAV in both numerical simulations and experiments against the PID controller. In addition, it offers an effective means to determine the gain parameters, which is similar to that of a conventional PID controller. Finally, the comparison results showed better performance in terms of robustness to disturbances in attitude and position control and tracking the desired trajectory at a higher frequency. It is important to release the assumption of disturbance for convergence time derivation in practice and it can be developed in future work.

REFERENCES

[1] A. Tayebi and S. McGilvray, "Attitude stabilization of a VTOL quadrotor aircraft," *IEEE Trans. Control Syst. Technol.*, vol. 14, no. 3, pp. 562–571, May 2006.

[2] X. Zhang, B. Xian, B. Zhao, and Y. Zhang, "Autonomous flight control of a nano quadrotor helicopter in a GPS-denied environment using on-board vision," *IEEE Trans. Ind. Electron.*, vol. 62, no. 10, pp. 6392–6403, Oct. 2015.

[3] R. C. Avram, X. Zhang, and J. Muse, "Quadrotor actuator fault diagnosis and accommodation using nonlinear adaptive estimators," *IEEE Trans. Control Syst. Technol.*, vol. 25, no. 6, pp. 2219–2226, Nov. 2017.

[4] R. C. Avram, X. Zhang, and J. Muse, "Nonlinear adaptive fault-tolerant quadrotor altitude and attitude tracking with multiple actuator faults," *IEEE Trans. Control Syst. Technol.*, vol. 26, no. 2, pp. 701–707, Mar. 2018.

[5] P. E. I. Pounds, D. R. Bersak, and A. M. Dollar, "Stability of small-scale UAV helicopters and quadrotors with added payload mass under PID control," *Auton. Robots*, vol. 33, nos. 1–2, pp. 129–142, 2012.

[6] D. Lee, H. J. Kim, and S. Sastry, "Feedback linearization vs. adaptive sliding mode control for a quadrotor helicopter," *Int. J. Control, Automat. Syst.*, vol. 7, no. 3, pp. 419–428, 2009.

[7] C. Li, Y. Zhang, and P. Li, "Full control of a quadrotor using parameter-scheduled backstepping method: Implementation and experimental tests," *Nonlinear Dyn.*, vol. 86, no. 2, pp. 1259–1278, Jul. 2017.

[8] D. Cabecinhas, R. Naldi, C. Silvestre, R. Cunha, and L. Marconi, "Robust landing and sliding maneuver hybrid controller for a quadrotor vehicle," *IEEE Trans. Control Syst. Technol.*, vol. 24, no. 2, pp. 400–412, Mar. 2016.

[9] K. Alexis, G. Nikolakopoulos, and A. Tzes, "Model predictive quadrotor control: Attitude, altitude and position experimental studies," *IET, Control Theory Appl.*, vol. 6, no. 12, pp. 1812–1827, Aug. 2012.

[10] T. Lee, "Robust adaptive attitude tracking on SO(3) with an application to a quadrotor UAV," *IEEE Trans. Control Syst. Technol.*, vol. 21, no. 5, pp. 1924–1930, Sep. 2013.

[11] Z. Zuo and S. Mallikarjunan, "L_1 Adaptive backstepping for robust trajectory tracking of UAVs," *IEEE Trans. Ind. Electron.*, vol. 64, no. 4, pp. 2944–2954, Apr. 2017.

[12] G. Antonelli, E. Cataldi, F. Arrichiello, P. R. Giordano, S. Chiaverini, and A. Franchi, "Adaptive trajectory tracking for quadrotor MAVs in presence of parameter uncertainties and external disturbances," *IEEE Trans. Control Syst. Technol.*, vol. 26, no. 1, pp. 248–254, Jan. 2018.

[13] L. Qiao and W. Zhang, "Double-loop integral terminal sliding mode tracking control for UUVs with adaptive dynamic compensation of uncertainties and disturbances," *IEEE J. Ocean. Eng.*, vol. 44, no. 1, pp. 29–53, Jan. 2019.

[14] L. Qiao and W. Zhang, "Adaptive second-order fast nonsingular terminal sliding mode tracking control for fully actuated autonomous underwater vehicles," *IEEE J. Ocean. Eng.*, vol. 44, no. 2, pp. 363–385, Apr. 2019.

[15] L. Wang and J. Su, "Robust disturbance rejection control for attitude tracking of an aircraft," *IEEE Trans. Control Syst. Technol.*, vol. 23, no. 6, pp. 2361–2368, Nov. 2015.

[16] H. Liu, D. Derawi, J. Kim, and Y. Zhong, "Robust optimal attitude control of hexarotor robotic vehicles," *Nonlinear Dyn.*, vol. 74, no. 4, pp. 1155–1168, Dec. 2013.

[17] B. Erginer and E. Altuğ, "Design and implementation of a hybrid fuzzy logic controller for a quadrotor VTOL vehicle," *Int. J. Control, Autom. Syst.*, vol. 10, no. 1, pp. 61–70, 2012.

[18] G. Nikolakopoulos and K. Alexis, "Switching networked attitude control of an unmanned quadrotor," *Int. J. Control, Automat. Syst.*, vol. 11, no. 2, pp. 389–397, 2013.

[19] X. Liu, L. Li, Z. Li, X. Chen, T. Fernando, H. H. C. Iu, and G. He, "Event-trigger particle filter for smart grids with limited communication bandwidth infrastructure," *IEEE Trans. Smart Grid*, vol. 9, no. 6, pp. 6918–6928, Nov. 2018.
[20] S. Li, L. Li, Z. Li, X. Chen, T. Fernando, H. H.-C. Iu, G. He, Q. Wang, and X. Liu, "Event-trigger heterogeneous nonlinear filter for wide-area measurement systems in power grid," *IEEE Trans. Smart Grid*, vol. 10, no. 3, pp. 2752–2764, May 2019.
[21] S. Li, Y. Hu, L. Zheng, X. Chen, T. Fernando, H. C. Lu, Q. Wang, and X. Liu, "Stochastic event-triggered cubature Kalman filter for power system dynamic state estimation," *IEEE Trans. Circuits Syst. II, Exp. Briefs*, vol. 66, no. 9, pp. 1552–1556, Sep. 2019.
[22] H. Bouadi, M. Bouchoucha, and M. Tadjine, "Sliding mode control based on backstepping approach for an UAV type-quadrotor," *World Acad. Sci., Eng. Technol.*, vol. 26, no. 5, pp. 22–27, 2007.
[23] F. Chen, R. Jiang, K. Zhang, B. Jiang, and G. Tao, "Robust backstepping sliding-mode control and observer-based fault estimation for a quadrotor UAV," *IEEE Trans. Ind. Electron.*, vol. 63, no. 8, pp. 5044–5056, Aug. 2016.
[24] H. Liu, W. Zhao, Z. Zuo, and Y. Zhong, "Robust control for quadrotors with multiple time-varying uncertainties and delays," *IEEE Trans. Ind. Electron.*, vol. 64, no. 2, pp. 1303–1312, Feb. 2017.
[25] H. Du and S. Li, "Finite-time attitude stabilization for a spacecraft using homogeneous method," *J. Guid., Control, Dyn.*, vol. 35, no. 3, pp. 740–748, 2012.
[26] Y. Wu, X. Yu, and Z. Man, "Terminal sliding mode control design for uncertain dynamic systems," *Syst. Control Lett.*, vol. 34, no. 5, pp. 281–287, 1998.
[27] S. Ding and S. Li, "Stabilization of the attitude of a rigid spacecraft with external disturbances using finite-time control techniques," *Aerosp. Sci. Technol.*, vol. 13, nos. 4–5, pp. 256–265, 2009.
[28] E. Jin and Z. Sun, "Robust controllers design with finite time convergence for rigid spacecraft attitude tracking control," *Aerosp. Sci. Technol.*, vol. 12, no. 4, pp. 324–330, 2008.
[29] J.-J. Xiong and E.-H. Zheng, "Position and attitude tracking control for a quadrotor UAV," *ISA Trans.*, vol. 53, no. 3, pp. 725–731, 2014.
[30] J.-J. Xiong and G.-B. Zhang, "Global fast dynamic terminal sliding mode control for a quadrotor UAV," *ISA Trans.*, vol. 66, pp. 233–240, Jan. 2017.
[31] W. Zhu, H. Du, Y. Cheng, and Z. Chu, "Hovering control for quadrotor aircraft based on finite-time control algorithm," *Nonlinear Dyn.*, vol. 88, no. 4, pp. 2359–2369, 2017.
[32] S. Ding, L. Liu, and W. Zheng, "Sliding mode direct yaw-moment control design for in-wheel electric vehicles," *IEEE Trans. Ind. Electron.*, vol. 64, no. 8, pp. 6752–6762, Aug. 2017.
[33] B. Xiao, Q. Hu, and Y. Zhang, "Finite-time attitude tracking of spacecraft with fault-tolerant capability," *IEEE Trans. Control Syst. Technol.*, vol. 23, no. 4, pp. 1338–1350, Jul. 2015.
[34] J. Wang, C. Zhang, S. Li, J. Yang, and Q. Li, "Finite-time output feedback control for PWM-based DC-DC buck power converters of current sensorless mode," *IEEE Trans. Control Syst. Technol.*, vol. 25, no. 4, pp. 1359–1371, Jul. 2017.
[35] H. Wang, X.-L. Zhang, X.-H. Wang, and X.-J. Zhu, "Finite time chaos control for a class of chaotic systems with input nonlinearities via TSM scheme," *Nonlinear Dyn.*, vol. 69, no. 4, pp. 1941–1947, 2012.
[36] R. R. Nair, L. Behera, and S. Kumar, "Event-triggered finite-time integral sliding mode controller for consensus-based formation of multirobot systems with disturbances," *IEEE Trans. Control Syst. Technol.*, vol. 27, no. 1, pp. 39–47, Jan. 2019, doi: 10.1109/TCST.2017.2757448.
[37] H. L. N. N. Thanh and S. K. Hong, "Quadcopter robust adaptive second order sliding mode control based on PID sliding surface," *IEEE Access*, vol. 6, pp. 66850–66860, 2018.
[38] A. Modirrousta and M. Khodabandeh, "Adaptive non-singular terminal sliding mode controller: New design for full control of the quadrotor with external disturbances," *Trans. Inst. Meas. Control*, vol. 39, no. 3, pp. 371–383, 2017.
[39] F. Muñoz, I. González-Hernández, S. Salazar, E. S. Espinoza, and R. Lozano, "Second order sliding mode controllers for altitude control of a quadrotor UAS: Real-time implementation in outdoor environments," *Neurocomputing*, vol. 232, no. 12, pp. 61–71, 2017.

WONMO CHUNG received the B.S. degree in mechanical and nuclear engineering from the Ulsan National Institute of Science and Technology (UNIST), Ulsan, South Korea, in 2016, where he is currently pursuing the Ph.D. degree with the School of Mechanical, Aerospace and Nuclear Engineering. His research interests include robust control of UAV, magnetic sensors, and magnetic induction tomography.

DIPAK KUMAR GIRI received the Ph.D. degree in spacecraft dynamics and control from the Indian Institute of Technology, Kharagpur. He was a Postdoctoral Research Associate with the Singapore-Massachusetts Institute of Technology (MIT), the Alliance for Research and Technology (SMART), and the Ulsan National Institute of Science and Technology (UNIST). He was an Erasmus Mundus Fellow with the Department of Electrical and Electronics Engineering, Middle East Technical University, Ankara, Turkey. He is currently a DST Inspire Faculty with the Department of Aerospace Engineering, IIT at Kanpur. His research interests include the areas of spacecraft dynamics and control, linear and non-linear control of dynamical systems, automatic control of spacecraft, system dynamics and trade space exploration models for designing complex aerospace systems and space exploration-on-orbit servicing, space debris removal, and orbital infrastructure design in LEO, MEO, and GEO.

HUNGSUN SON (S'07–M'09) received the M.S. degree in aero and astronautical engineering from Stanford University, Stanford, CA, USA, in 2002, and the Ph.D. degree in mechanical engineering from the Georgia Institute of Technology, Atlanta, in 2007. He is currently an Associate Professor of mechanical, aerospace and nuclear engineering, Ulsan National Institute of Science and Technology (UNIST), South Korea. His current research interests include mechatronics, sensors and actuators, dynamic system modeling, design optimization, automation, and control.